Available online at www.sciencedirect.com
ScienceDirect
Journal of the European Ceramic Society 29 (2009) 67–75
www.elsevier.com/locate/jeurceramsoc

# Diffraction, structure and phase stability studies on aluminium titanate

R.D. Skala [a], D. Li, I.M. Low *

*Centre for Materials Research, Department of Applied Physics, Curtin University of Technology, GPO Box U1987, Perth, WA 6845, Australia*

Received 21 March 2008; received in revised form 26 May 2008; accepted 30 May 2008
Available online 14 July 2008

**Abstract**

The crystal structure studies of aluminium titanate ($Al_2TiO_5$) in the temperature range of 25–1200 °C have been investigated by X-ray and neutron powder diffraction. The use of simultaneous refinement of the X-ray and neutron data has enhanced the refinement precision of the structure model of $Al_2TiO_5$ with the concomitant improvement in values such as atomic coordinates, site occupancies and unit-cell parameters. Results from Rietveld refinements showed that the disordering of Ti and Al atoms in the metal 1 and metal 2 sites. High-temperature neutron diffraction studies of the $Al_2TiO_5$ crystal structure revealed an increasing substitution of Al for the Ti atoms in the crystal structure. It is proposed that this increased substitution is responsible for the decomposition of $Al_2TiO_5$ that is observed between 900 and 1280 °C.


*Keywords:* Sintering; X-ray methods; Thermal properties; $Al_2TiO_5$; Refractories

## 1. Introduction

Aluminium titanate ($Al_2TiO_5$) is an excellent refractory and thermal shock resistant material due to its relatively low thermal expansion coefficient ($\sim 1 \times 10^{-6}\,°C^{-1}$) and high melting point (1860 °C). It is these properties that make $Al_2TiO_5$ suitable for high-temperature applications where thermal shock resistance and thermal insulation is required, such as components of internal combustion engines, exhaust port liners, metallurgy, and thermal barriers.[1–4]

$Al_2TiO_5$ is one of several materials which is isomorphous with the mineral pseudobrookite ($Fe_2TiO_5$).[5–8] In this structure, each $Al^{3+}$ or $Ti^{4+}$ cation is surrounded by six oxygen ions forming distorted oxygen octahedra. These $AlO_6$ or $TiO_6$ octahedra form ⟨0 0 1⟩ oriented double chains weakly bonded by shared edges. This structural feature is responsible for the strong thermal expansion anisotropy which generates localised internal stresses to cause severe microcracking. Although this microcracking weakens the material, it imparts a desirable low thermal expansion coefficient and an excellent thermal shock resistance. In addition, $Al_2TiO_5$ is only thermodynamically stable above 1280 °C and undergoes a eutectoid-like decomposition to α-$Al_2O_3$ and $TiO_2$ (rutile) within the temperature range of 900–1280 °C.[9–20] The eutectoid decomposition occurs at 1280 °C (equilibrium), but takes place upon undercooling.[10] This thermal behaviour of $Al_2TiO_5$ is due primarily to the complex system of internal stresses and fractures that develop in the material during cooling from elevated temperatures, and thus are the result of the anisotropic structural properties of individual grains which form the bulk of the ceramic body.[6,9,10]

Early crystal structure studies of $Al_2TiO_5$ by Austin and Schwartz[5] established that the crystal structure is isomorphous with the mineral pseudobrookite ($Fe_2TiO_5$) which crystallizes in the orthorhombic symmetry with space-group *Bbmm*. Both structures are differentiated only by small differences in the atomic coordinates of the constituent atoms. $Al_2TiO_5$ crystallises as an orthorhombic unit-cell in the *Cmcm* (no. 63) space-group (using a *c*-face centred unit-cell) with lattice parameters of $a = 3.557$ Å, $b = 9.436$ Å, and $c = 9.648$ Å. The structure of $Al_2TiO_5$ consists of distorted edge-shared oxygen [$MeO_6$] octahedra surrounding the metal sites, M1 and M2 which have a coordination number of 6. The metal atoms exist on fourfold (4c) symmetry sites and the oxygen atoms on eightfold (8f) symmetry sites.[6] The crystal structure of $Al_2TiO_5$ is shown in Fig. 1. The distorted octahedra are clearly seen to be linked by edge sharing in the *b* and *c* lattice directions and apex sharing in the *a*-direction.

* Corresponding author. Tel.: +61 8 9266 7544; fax: +618 9266 2377.
*E-mail address:* j.low@curtin.edu.au (I.M. Low).
[a] Current address: Millennium Chemicals Inc., 6752 Baymeadow Drive, Glen Burnie, MD 21060, USA.

0955-2219/$ – see front matter. 
doi:10.1016/j.jeurceramsoc.2008.05.037

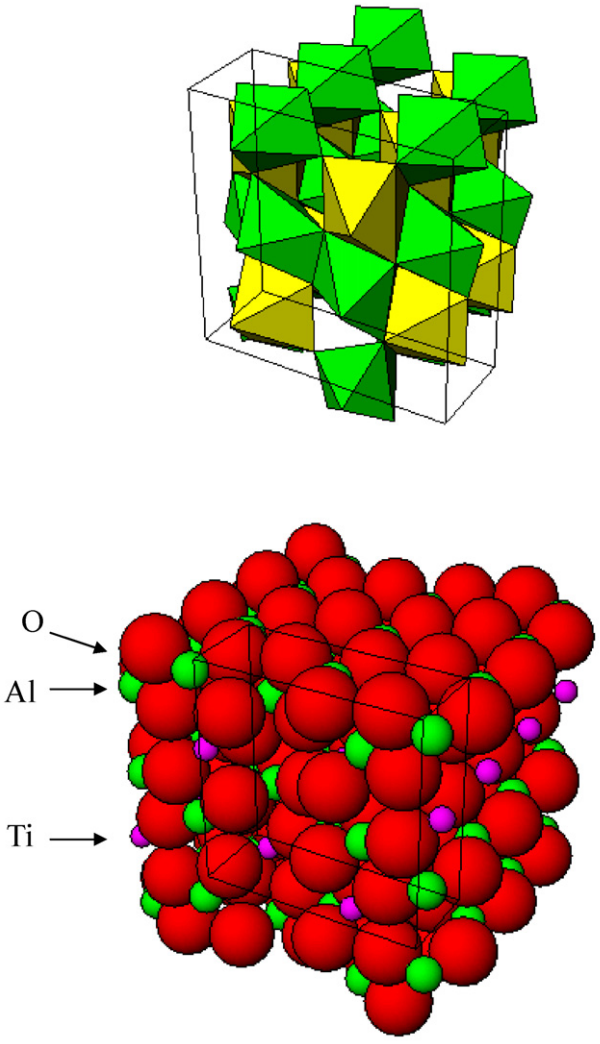


Fig. 1. Conventional crystal structure of $Al_2TiO_5$ showing both the (a) distorted, edge-shared oxygen octahedra about each metal site and (b) the oxygen–metal bonds (green: Al, purple: Ti, red: O). The square structure on each image is the outline of a single unit-cell. (For interpretation of the references to colour in this figure legend, the reader is referred to the web version of the article.)

Hitherto, the crystal structure of $Al_2TiO_5$ has not been well researched and the literature models have not fitted the measured data very well. Discrepancies in the peak positions and/or peak intensities were found to exist between the models available and the measured data in this work. There is thus a need to improve on the exiting models for the crystal structure of $Al_2TiO_5$ in terms of atomic coordinates, site occupancies and unit-cell parameters which are essential for the accurate determination of quantitative phase abundances from the Rietveld analysis of diffraction data in a multi-phase $Al_2TiO_5$-based system. In addition, the relationship between the variations of lattice constants and the thermal stability of $Al_2TiO_5$ at elevated temperatures is not fully understood. Similarly, the effect of temperature on the atomic positional coordinates and on the site occupancies of the metal atoms within the crystal structure remains poorly understood.

## 2. Experimental procedure

### 2.1. Sample preparation

Aluminium titanate was synthesised from α-alumina and rutile. Equimolar mixtures of $Al_2O_3$ (A1000SG, ALCOA, USA; particle size: ∼1.0 μm) and $TiO_2$ (SCM Chemicals, Bunbury, West Aust.; particle size: ∼1.0 μm) were wet-milled together for 4 h in an attrition mill to obtain an intimate mix and also to reduce the particle size in order to enhance the rate of the solid-state reaction. After drying, the mixed powder was placed in an α-alumina crucible and sintered in air at 1550 °C for 4 h. The resulting powder was then examined using X-ray diffraction (XRD) to confirm the formation of $Al_2TiO_5$. This sintering step was repeated a number of times in an attempt to reduce the amount of residual α-alumina and rutile in the $Al_2TiO_5$ powder due to an incomplete reaction. After four such sintering runs, the XRD pattern of the powder showed that it was predominately $Al_2TiO_5$ with minor phases of α-alumina and rutile according to the relatively close pattern matches with the ICDD powder diffraction cards, 41-258, 42-1468 and 21-1276 for $Al_2TiO_5$, α-alumina and rutile, respectively.

### 2.2. X-ray diffraction

X-ray diffraction patterns were collected on the samples for phase identification and analysis. A Siemens D500 diffractometer fitted with a Cu tube operating at 40 kV, 30 mA was used. The diffractometer using Bragg–Brentano geometry was fitted with a NaI scintillation detector and a graphite monochromator. The samples were mounted in aluminium sample holders and held in place with an adhesive (Blu-Tack, Bostick, Australia). Scans were taken over the $2\theta$ angular range of 10–100° with a step size of 0.04° and a counting time of 1.0 s at each step. Quantitative phase analysis was undertaken using the Rietveld pattern fitting method.

### 2.3. Pattern indexing and unit-cell refinement

The software PCPIRUM[21] was used to refine the unit-cell parameters and review the space-group of the crystal structure. Indexing of the XRD pattern using PCPIRUM, confirmed that the space-group of the crystal system is *Cmcm* (no. 63), with reflection conditions; $h\,k\,l$: $h+k=2n$ and $h\,0\,l$: $h=2n$, $l=2n$. The crystal unit-cell parameters, obtained from the literature, for $Al_2TiO_5$ were used as a starting model for PCPIRUM. The refined unit-cell parameters were $a=3.593(2)$ Å, $b=9.433(1)$ Å and $c=9.641(1)$ Å. The figures of merit[22,23] were found to be, $M_{20}=14$ and $F_{20}=15$ (0.027, 49).

### 2.4. Rietveld refinement of X-ray diffraction data

The diffraction patterns were re-collected using a smaller step size (0.02°) and longer counting time (4 s) to improve the counting statistics of the data. The data was analysed using LHPM.[24] A pseudo-Voight function was used to model the shape of the diffraction peaks. All parameters of interest including

background, zero-point, scale factors for all phases, half-width, asymmetry parameters, preferred orientation, unit-cell parameters, atomic positional coordinates, temperature factors and in the case of neutron data site occupancies of the metal atoms were refined step-by-step for avoiding correlations. The starting positional parameters and temperature factors, as reported by Morosin and Lynch[6] for $Al_2TiO_5$, were transformed to the standard setting, *Cmcm* (no. 63).[25]

### 2.5. Neutron diffraction (ND)

$Al_2TiO_5$ powder (>98% purity) was also analysed using the high-resolution powder diffractometer (HRPD) for complimentary crystal structure information to the XRD study conducted. Thermal neutrons of wavelength $\lambda = 1.493$ Å were used with a $2\theta$ angular scan range of 5–155°, at a step size of 0.05° and a monitor count of 100,000 (approximately 36 s counting time/step) with the powder sample contained in a 16-mm diameter vanadium can.

The same $Al_2TiO_5$ powder sample was also run on the medium resolution powder diffractometer (MRPD) for structure studies at high temperature. The powder was contained in a 16-mm stainless steel (type 253MA) can and surrounded by an alumina tube furnace with $MoSi_2$ heating elements (Ceramic Engineering). ND patterns for the powder sample were obtained at 25, 400, 800 and 1200 °C. In this phase of study, thermal neutrons were used with a wavelength, $\lambda = 1.664$ Å. The patterns were collected over the angular range of 5–135° with a step size of 0.1°, and a monitor count of 70,000 (approximately 25 s/step).

### 2.6. Rietveld refinement of neutron diffraction data

The ND data was analysed using the same software packages as previously used for the X-ray analysis. The use of neutrons for the analysis of the sample proved to be complimentary to the X-ray source used previously. XRD occurs, primarily, through the interaction of the incident X-ray beam with the electrons of the constituent atoms. As such, the scattering factors for the X-ray beam are simply proportional to the atomic number of the elements within the sample. It is this feature which makes it difficult to distinguish the atoms for which the atomic numbers are relatively close together. The mechanism of neutron scattering, on the other hand is fundamentally different. The incident neutrons are scattered by atomic nuclei. The underlying mechanism of scattering by atomic nuclei is a combination of potential and resonance scattering which leads to scattering lengths that vary irregularly across the periodic table. The neutron scattering lengths for Al and Ti are 0.35 and $-0.34 \times 10^{-12}$ cm, respectively. Therefore, these atoms are relatively easy to distinguish from one another. As a consequence of this, the refinement of the site occupancies of the Al and Ti atoms using ND was expected to be more reliable than using XRD.

The structure of $Al_2TiO_5$, that was previously optimised using XRD, was used as a starting model for the refinement of the ND data. All possible parameters were varied during the refinement process, including the site occupancies of the metal atoms. The occupancies of the oxygen atoms were not refined and were adjusted to balance the overall charge of the crystal to maintain neutrality.

## 3. Results

### 3.1. Rietveld refinement of X-ray diffraction data

The XRD pattern of synthesized powder displays a high concentration of $Al_2TiO_5$. Residual α-alumina and rutile are also present in the sample most probably due to spontaneous decomposition of $Al_2TiO_5$ during furnace cooling to room temperature. Calculation of the phase abundances from the scale factors obtained from the Rietveld refinement of the diffraction data confirms that the $Al_2TiO_5$ is the major phase, with the minor phases being α-alumina and rutile. The crystalline phase concentrations were normalised to 100% and were determined to be $94.1 \pm 0.8$ wt.% $Al_2TiO_5$, $5.2 \pm 0.1$ wt.% α-alumina and $0.7 \pm 0.1$ wt.% rutile.

The results of this work are shown in Table 1. The initial starting values used, and those of Morosin and Lynch[6] are also shown. For comparative purposes, the atomic coordinates reported by Morosin and Lynch has been transformed to *Cmcm* setting. The slight discrepancies between the atomic coordinates reported by Morosin and Lynch and those of this study can be mainly attributed to the different sample preparation techniques employed which also resulted in the differences observed in the site occupancies of the cation atoms. In addition, a single crystal of $Al_2TiO_5$ was used by Morosin and Lynch, whereas a multi-phase powder sample was used in this study. The multi-phase refinement strategy employed in this study may also have a higher chance of correlation between the parameters varied; to bias the final positional parameters determined from the Rietveld refinement. The values obtained for the atomic coordinates in this study are in relatively good agreement with those of Morosin and Lynch.

Fig. 2 shows a typical pattern plot after refinement of all parameters of interest. The calculated pattern is overlaid on the measured pattern and the differences between two profiles are plotted along the bottom. From the refinement results, the *R* parameters were found to suggest a relatively accurate refinement. The GOF is an overall measure of the match between the

Table 1
Refined atomic coordinates for $Al_2TiO_5$ from XRD data and Morosin and Lynch[6]

| Atom | This study | | | Morosin & Lynch[a] | | |
|---|---|---|---|---|---|---|
| | *x* | *y* | *z* | *x* | *y* | *z* |
| Ti1 | 0 | 0.1883 (8) | 0.25 | 0 | 0.1854 (1) | 0.25 |
| Al1 | 0 | 0.1883 (8) | 0.25 | 0 | 0.1854 (1) | 0.25 |
| Ti2 | 0 | 0.1373 (7) | 0.5645 (8) | 0 | 0.1348 (1) | 0.5615 (1) |
| Al2 | 0 | 0.1373 (7) | 0.5645 (8) | 0 | 0.1348 (1) | 0.5615 (1) |
| O1 | 0 | 0.7618 (9) | 0.25 | 0 | 0.7577 (3) | 0.25 |
| O2 | 0 | 0.0359 (8) | 0.1063 (7) | 0 | 0.0485 (2) | 0.1167 (2) |
| O3 | 0 | 0.3142 (7) | 0.0681 (5) | 0 | 0.3125 (2) | 0.0721 (2) |

$R_p = 13.12$, $R_{wp} = 17.97$, $R_{exp} = 5.87$, GOF = 9.54.

[a] Atomic coordinates transformed from *Bbmm* space-group to *Cmcm* space-group used in this study.[26]

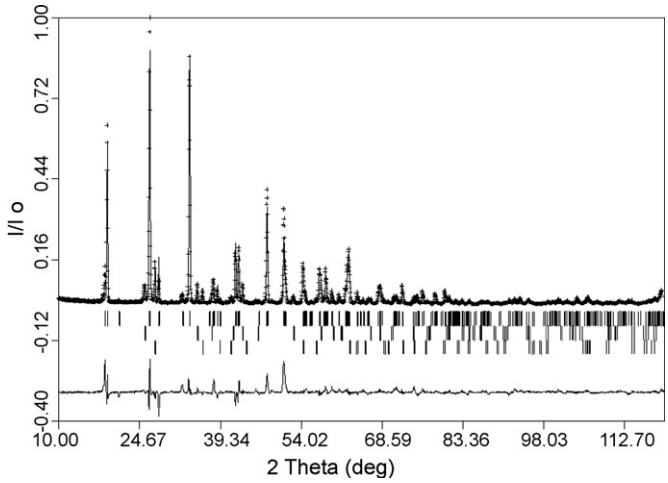


Fig. 2. XRD profile plot of $Al_2TiO_5$ powder after Rietveld refinement. Measured pattern indicated by crosses, calculated pattern indicated by solid line. Intensity differences between the two patterns are shown along the bottom of the plot. Vertical bars represent the allowable peak positions for each of the phases, $\lambda = 1.5406$ Å (top: $Al_2TiO_5$, middle: $Al_2O_3$, lower: $TiO_2$).

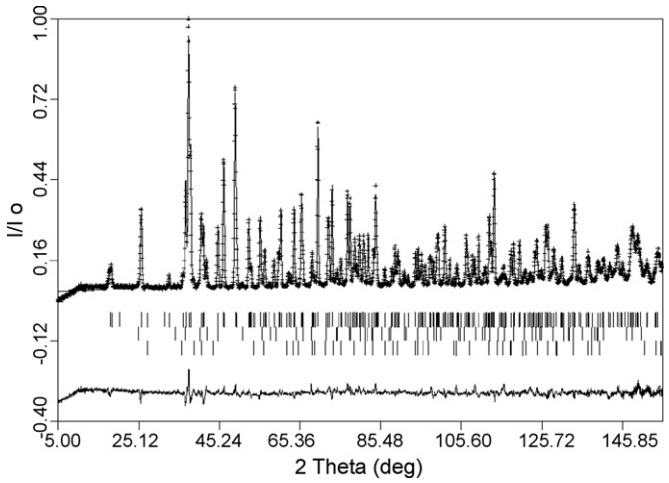


Fig. 3. Neutron diffraction profile plot of $Al_2TiO_5$ powder after Rietveld refinement. Measured pattern indicated by crosses, calculated pattern indicated by solid line. Intensity differences between the two patterns are shown along the bottom of the plot. Vertical bars represent the allowable peak positions for each of the phases, $\lambda = 1.493$ Å (top: $Al_2TiO_5$, middle: $Al_2O_3$, lower: $TiO_2$).

measured and calculated patterns. The relatively high value for the GOF, in this case, could be related to the conditions employed during data collection.

### 3.2. Rietveld refinement of neutron diffraction data

Table 2 shows the refined atomic coordinates from the ND study of $Al_2TiO_5$. Fig. 3 shows the resulting diffraction pattern after the refinement has been completed. The calculated pattern is overlaid on the measured pattern and a difference plot is generated. The difference plot can be used as a qualitative measure of the goodness-of-fit of the calculated pattern, obtained from the refined crystal structure model, to the measured data.

### 3.3. Simultaneous Rietveld refinement of X-ray and neutron diffraction data

In order to yield a more precise structure and elucidate the extent of cation substitution, a simultaneous Rietveld refinement of both the XRD and ND data was conducted. The result of this refinement is a more precise structural determination to date and provides a better understanding of disordering for both metal sites. The complete structure parameter listing for $Al_2TiO_5$ from this simultaneous refinement is given in Table 3.

Table 2
Refined atomic coordinates for $Al_2TiO_5$ from neutron diffraction data

| Atom | *x* | *y* | *z* |
|---|---|---|---|
| Ti1 | 0 | 0.1897 (6) | 0.25 |
| Al1 | 0 | 0.1897 (6) | 0.25 |
| Ti2 | 0 | 0.1427 (5) | 0.5585 (6) |
| Al2 | 0 | 0.1427 (5) | 0.5585 (6) |
| O1 | 0 | 0.7568 (3) | 0.25 |
| O2 | 0 | 0.0483 (3) | 0.1167 (2) |
| O3 | 0 | 0.3122 (3) | 0.0725 (2) |

$R_p = 5.23$, $R_{wp} = 6.52$, $R_{exp} = 2.57$, GOF = 6.45.

The results from this simultaneous refinement are believed to represent an accurate structure model for $Al_2TiO_5$. The standard deviations associated with each value are much smaller than previously which indicates that the refinement precision of the structure model and values such as atomic coordinates, site occupancies and unit-cell parameters have improved. Fig. 4 shows the diffraction patterns after simultaneous refinement of the X-ray and neutron data.

### 3.4. Interatomic distances and bond angles

The interatomic distances and angles, calculated from the refined structure parameters,[27] are shown in Table 4. The two metal sites M1 (Ti, Al) and M2 (Ti, Al) have octahedral coordination, with each site surrounded by six oxygen atoms. This is not clearly indicated by Morosin and Lynch. In considering the angles between the oxygen atoms on the plane of the metal atom, the structure can be considered a distorted octahedra. This is evident for both metal sites and is in agreement with the results obtained by Morosin and Lynch. The angles between the oxygen atoms at the vertices of the octahedra and the metal atom also show a distortion for both octahedra.

Table 3
Final structure parameters for $Al_2TiO_5$ from simultaneous refinement of X-ray and neutron diffraction data

| Atom | Site | *x* | *y* | *z* | B | N |
|---|---|---|---|---|---|---|
| Ti1 | 4c | 0 | 0.1881 (4) | 0.25 | 1.59 (9) | 0.412 (3) |
| Al1 | 4c | 0 | 0.1881 (4) | 0.25 | 1.59 (9) | 0.588 (3) |
| Ti2 | 8f | 0 | 0.1370 (3) | 0.5614 (3) | 1.17 (4) | 0.288 (4) |
| Al2 | 8f | 0 | 0.1370 (3) | 0.5614 (3) | 1.17 (4) | 0.712 (4) |
| O1 | 4c | 0 | 0.7572 (2) | 0.25 | 0.48 (4) | |
| O2 | 8f | 0 | 0.0481 (2) | 0.1164 (2) | 0.66 (2) | |
| O3 | 8f | 0 | 0.3120 (2) | 0.0718 (2) | 0.58 (2) | |

$R_p = 9.56$, $R_{wp} = 9.79$, GOF = 16.40.

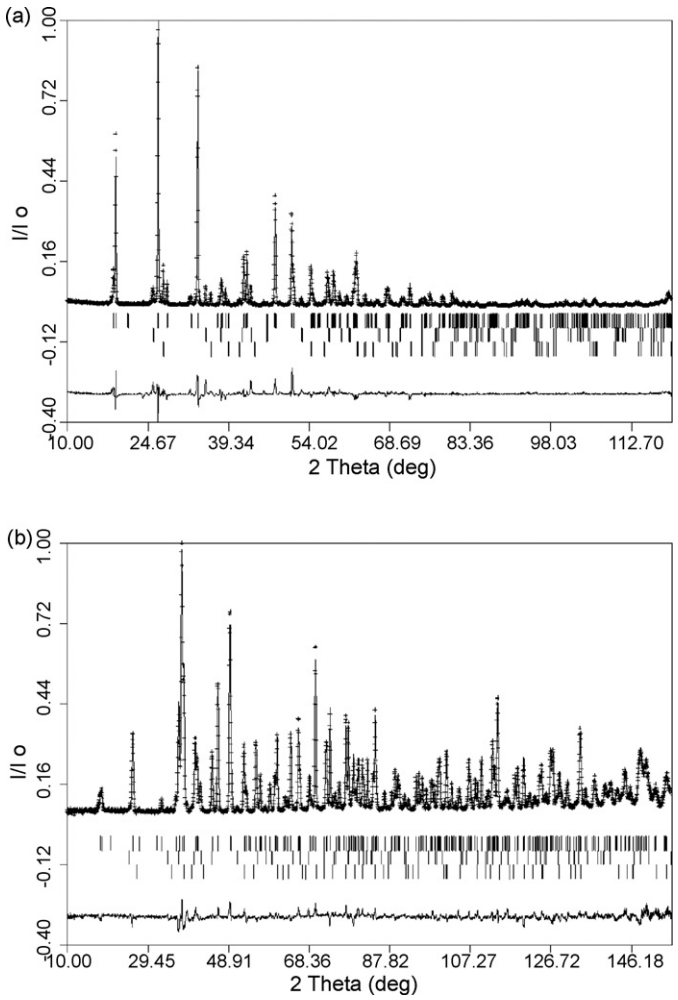


Fig. 4. Diffraction patterns of $Al_2TiO_5$ after simultaneous refinement of X-ray and neutron data. Upper pattern represents the X-ray dataset and the lower represents the neutron dataset. (Top: $Al_2TiO_5$, middle: $Al_2O_3$, lower: $TiO_2$).

The structure parameters show that both Ti and Al atoms have a disordered distribution on the sites, M1 (4c) and M2 (8f) in the structure. The site occupancies of Ti and Al are 41.2% and 58.8% on the M1 (4c) and 28.8% and 71.2% on the M2 (8f) sites, respectively. These values deviate from the values published by Morosin and Lynch which are similar for both the M1 and M2 sites of 33.3% Ti and 66.7% Al. These discrepancies in the site occupancies for both the Ti and Al atoms between this study and that of Morosin and Lynch may be attributed to the sample preparation method and purity of the sample used.

Fig. 5 shows the crystal structure of $Al_2TiO_5$ determined from this study. The octahedral with the two edges shared are clearly visible. The octahedra themselves are distorted, with the oxygen atoms ($O1_1$, $O1_2$ for M1 and $O3_2$, $O3_3$ for M2) at the vertices of each polyhedra shifted slightly from directly above the metal atom. The four oxygen atoms ($O2_1$, $O2_2$, $O3_1$, $O3_2$ and $O1_1$, $O2_1$, $O2_2$, $O3_1$ for the M1 and M2 sites, respectively) which form the plane around the metal atom are also distorted, as shown by the figure and the values for the angles between the oxygens and the metal atom (Table 4).

Table 4
Interatomic distances and angles for $Al_2TiO_5$

| Polyhedra 1 | Å | Polyhedra 2 | Å |
|---|---|---|---|
| $M1–O1_1$ | 1.861 (2) | $M2–O1_1$ | 2.015 (3) |
| $M1–O1_2$ | 1.861 (2) | $M2–O2_1$ | 1.869 (3) |
| $M1–O2_1$ | 1.893 (3) | $M2–O2_2$ | 1.943 (3) |
| $M1–O2_2$ | 1.893 (3) | $M2–O3_1$ | 2.081 (3) |
| $M1–O3_1$ | 2.019 (3) | $M2–O3_2$ | 1.833 (7) |
| $M1–O3_2$ | 2.019 (3) | $M2–O3_3$ | 1.833 (7) |
| $O1_1–O2_1$ | 2.954 (2) | $O3_2–O1_1$ | 2.531 (2) |
| $O1_1–O2_2$ | 2.954 (2) | $O3_2–O3_1$ | 2.552 (2) |
| $O1_1–O3_1$ | 2.531 (1) | $O3_2–O2_1$ | 2.893 (2) |
| $O1_1–O3_2$ | 2.531 (1) | $O3_2–O2_2$ | 2.854 (2) |
| $O1_2–O2_1$ | 2.954 (2) | $O3_3–O1_1$ | 2.531 (2) |
| $O1_2–O2_2$ | 2.954 (2) | $O3_3–O3_1$ | 2.552 (2) |
| $O1_2–O3_1$ | 2.531 (1) | $O3_3–O2_1$ | 2.893 (2) |
| $O1_2–O3_2$ | 2.531 (1) | $O3_3–O2_2$ | 2.854 (2) |
| $O2_1–O2_2$ | 2.579 (3) | $O2_1–O1_1$ | 3.031 (2) |
| $O2_1–O3_1$ | 2.524 (3) | $O1_1–O3_1$ | 3.161 (2) |
| $O2_2–O3_2$ | 2.524 (3) | $O3_1–O2_2$ | 2.524 (3) |
| $O3_2–O3_1$ | 3.425 (3) | $O2_2–O2_1$ | 2.411 (3) |
| $O2_1–M1–O2_2$ | 86.59 (3)° | $O2_2–M2–O2_1$ | 80.78 (3)° |
| $O2_2–M1–O3_2$ | 81.90 (3)° | $O2_1–M2–O1_1$ | 97.82 (3)° |
| $O3_2–M1–O3_1$ | 104.51 (3)° | $O1_1–M2–O3_1$ | 98.39 (2)° |
| $O3_1–M1–O2_1$ | 82.90 (3)° | $O3_1–M2–O2_2$ | 81.35 (2)° |
| $O1_1–M1–O1_2$ | 115.13 (3)° | $O3_2–M2–O3_3$ | 117.29 (5)° |

Values in parentheses indicate estimated standard deviations. Space-group *Cmcm*.

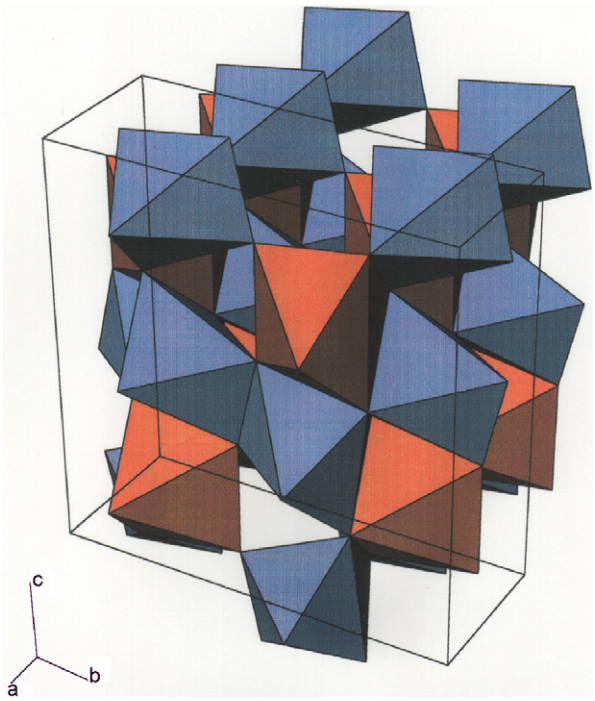


Fig. 5. Crystal structure of $Al_2TiO_5$ showing distorted edge-shared octahedra about each metal site. Metal 1 octahedra coloured orange, metal 2 octahedra coloured blue. Oxygen atoms are located on the vertices of each octahedra. Unit-cell represented by the box on the image. (For interpretation of the references to colour in this figure legend, the reader is referred to the web version of the article.)

### 3.5. High-temperature neutron diffraction

Rietveld analysis of the high-temperature diffraction was performed to observe the effect of temperature on the atomic positional coordinates and on the site occupancies of the metal atoms within the structure. The results of these analyses are shown in Table 5. From the results, it can be seen that for the M1 site, there is a significant decrease in the atomic positional coordinates as the temperature increases from room temperature to 400 °C. However, as the temperature increases from 800 to 1200 °C, the positional coordinates remain relatively constant. The *y* positional coordinate of the M2 site remains constant over the temperature range studied. However, the *z* positional coordinate is seen to decrease over the same temperature range. The coordinates for the O1, O2 and O3 oxygens are also found to remain constant within the range of uncertainties associated with the values. It was unexpected that the atomic positional coordinates of the oxygen atoms were less influenced by temperature than those of the metal sites. A marginal decrease in the *y* coordinate of the O1 site was observed when the temperature was increased to 800 °C, also a slight increase in the *y* coordinate of the O2 site occurred between 800 and 1200 °C. The coordinates of the O3 site were seen to remain relatively constant over the temperature range studied. The important point to note about these results, are the site occupancies of the cations on the M1 and M2 sites. As the temperature increases, it is seen that the site occupancies of the Al atoms within the M1 and M2 sites increased. The site occupancy of Al on the M1 site increases from 65.2% at room temperature (20 °C) to 71.5% at 1200 °C. A similar trend is also seen with the Al atoms in the M2 site, with an increase from 69.4% at room temperature to 73.3% at 1200 °C.

The largest increase in site occupancies of Al for both the M1 and M2 sites occurs when the temperature increases from 800 to 1200 °C. This temperature range is also the range in which $Al_2TiO_5$ decomposes into its constituent phases, namely α-alumina and rutile.

During the refinement of the neutron datasets, the unit-cell parameters were also refined. This allows an assessment of the variation of unit-cell parameters as a function of temperature. The results were plotted and a line of best-fit fitted to each of the datasets. The gradient of this line of best-fit allows the determination of the thermal expansion coefficient in each of the three crystallographic directions. The results of this are shown in Fig. 6.

Table 6 shows the results from this work when compared to those of other researchers. It can be seen that the results for the thermal expansion coefficients for this work compares favourably with those of Morosin and Lynch,[6] Buessem and Gruver[28] Bayer[29] and Freudenberg.[30] The results show that the $Al_2TiO_5$ crystal contracts during heating in the *a* lattice

Table 5
Atomic coordinates and occupancy factors for $Al_2TiO_5$ at room temperature, 400, 800 and 1200 °C

| Atom | RT[a] | | | | 400 °C[b] | | | |
|---|---|---|---|---|---|---|---|---|
| | *x* | *y* | *z* | *N* | *x* | *y* | *z* | *N* |
| Ti1 | 0 | 0.1986 (5) | 0.25 | 0.348 (4) | 0 | 0.1793 (6) | 0.25 | 0.332 (4) |
| Al1 | 0 | 0.1986 (5) | 0.25 | 0.652 (4) | 0 | 0.1793 (6) | 0.25 | 0.668 (4) |
| Ti2 | 0 | 0.1438 (3) | 0.5646 (3) | 0.306 (3) | 0 | 0.1446 (4) | 0.5621 (3) | 0.314 (4) |
| Al2 | 0 | 0.1438 (3) | 0.5646 (3) | 0.694 (3) | 0 | 0.1446 (4) | 0.5621 (3) | 0.686 (4) |
| O1 | 0 | 0.7568 (1) | 0.25 | | 0 | 0.7547 (2) | 0.25 | |
| O2 | 0 | 0.0485 (1) | 0.1157 (1) | | 0 | 0.0483 (2) | 0.1162 (1) | |
| O3 | 0 | 0.3129 (1) | 0.0719 (1) | | 0 | 0.3131 (2) | 0.0716 (1) | |
| *a* | | | 3.5823 (4) | | | | 3.5795 (4) | |
| *b* | | | 9.4062 (4) | | | | 9.4499 (5) | |
| *c* | | | 9.6134 (4) | | | | 9.6881 (5) | |
| Atom | 800 °C[c] | | | | 1200 °C[d] | | | |
| | *x* | *y* | *z* | N | *x* | *y* | *z* | *N* |
| Ti1 | 0 | 0.1733 (8) | 0.25 | 0.322 (6) | 0 | 0.1711 (9) | 0.25 | 0.285 (7) |
| Al1 | 0 | 0.1733 (8) | 0.25 | 0.678 (6) | 0 | 0.1711 (9) | 0.25 | 0.715 (7) |
| Ti2 | 0 | 0.1409 (7) | 0.5607 (6) | 0.303 (7) | 0 | 0.1419 (8) | 0.5534 (8) | 0.267 (6) |
| Al2 | 0 | 0.1409 (7) | 0.5607 (6) | 0.697 (7) | 0 | 0.1419 (8) | 0.5534 (8) | 0.733 (6) |
| O1 | 0 | 0.7527 (2) | 0.25 | | 0 | 0.7519 (4) | 0.25 | |
| O2 | 0 | 0.0489 (2) | 0.1159 (2) | | 0 | 0.0509 (3) | 0.1152 (3) | |
| O3 | 0 | 0.3118 (2) | 0.0713 (3) | | 0 | 0.3120 (4) | 0.0726 (3) | |
| *a* | | | 3.5744 (5) | | | | 3.5700 (6) | |
| *b* | | | 9.4872 (6) | | | | 9.5415 (7) | |
| *c* | | | 9.7621 (6) | | | | 9.8512 (7) | |

[a] $R_p = 3.87$, $R_{wp} = 4.43$, GOF = 3.16.
[b] $R_p = 4.13$, $R_{wp} = 4.84$, GOF = 3.84.
[c] $R_p = 3.74$, $R_{wp} = 4.38$, GOF = 3.17.
[d] $R_p = 4.00$, $R_{wp} = 4.83$, GOF = 3.97.

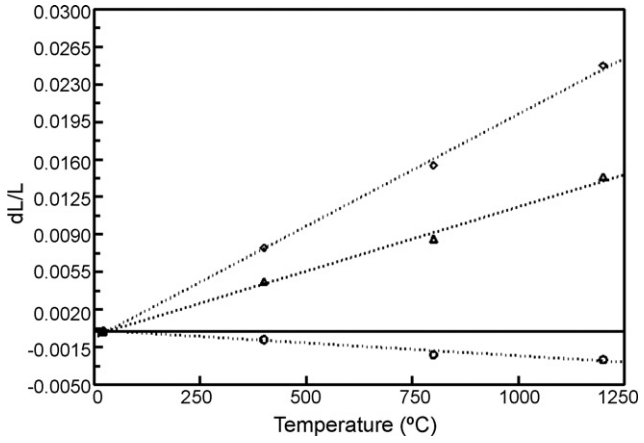


Fig. 6. Variation of unit-cell parameters of $Al_2TiO_5$ as a function of temperature. Dashed lines represent lines of best fit for each dataset. (◯) d*a*/*a*, (△) d*b*/*b* and (◇) d*c*/*c*.

direction, and expands in the other two directions, *b* and *c*, at different rates.

The results of the analysis of the interatomic distances and angles for the high-temperature ND data are summarised in Tables 7 and 8. From these results it can be clearly seen that as the temperature is increased, the distortion of the octahedra, about the M1 site becomes more pronounced, whereas the distortion about the M2 octahedra remains more or less constant. Furthermore, as the temperature is increased, the site occupancies of Al on the M1 and M2 sites increased. This implies that no decomposition of $Al_2TiO_5$ at high temperature had taken place because the same crystal structure was maintained only substitutional sites have been changed. However, the changes in Al and Ti sites indicate that these are pre-eutectoid changes at the atomic scale that may enhance subsequent eutectoid decomposition.

From the results presented in Tables 7 and 8, the bond lengths between the M1 and O sites and the M2 and O sites were also seen to increase with increasing temperature. This is then related to the increases in the *b* and *c* unit-cell parameters, as shown in Table 5. It can also be inferred that, due to the increases in the *b* and *c* unit-cell parameters, the volume of the unit-cell must also increase with increasing temperature.

## 4. Discussion

The crystal structure of $Al_2TiO_5$ has been successfully examined and characterised using the Rietveld refinement method.

Table 6
Thermal expansion coefficients obtained from neutron diffraction studies of $Al_2TiO_5$ powder at elevated temperatures

| $\alpha_a(\times10^{-6}\,K^{-1})$ | $\alpha_b(\times10^{-6}\,K^{-1})$ | $\alpha_c(\times10^{-6}\,K^{-1})$ | Reference |
|---|---|---|---|
| $-2.38\pm0.32$ | $11.97\pm0.60$ | $20.80\pm0.57$ | This study |
| 9.8 | 20.6 | −1.4 | [6] |
| 11.8 | 19.4 | −2.6 | [28] |
| −3.0 | 11.8 | 21.8 | [29] |
| −3.0 | 12.0 | 22.0 | [30] |

Table 7
Interatomic distances and angles for the M1 octahedra of $Al_2TiO_5$ at room temperature, 400, 800 and 1200 °C

| | Room temperature (Å) | 400 °C (Å) | 800 °C (Å) | 1200 °C Å |
|---|---|---|---|---|
| M1–$O1_1$ | 1.873 (2) | 1.926 (3) | 1.939 (3) | 1.947 (3) |
| M1–$O1_2$ | 1.873 (2) | 1.926 (3) | 1.939 (3) | 1.947 (3) |
| M1–$O2_1$ | 1.913 (2) | 1.792 (2) | 1.762 (2) | 1.755 (2) |
| M1–$O2_2$ | 1.913 (2) | 1.792 (2) | 1.762 (2) | 1.755 (2) |
| M1–$O3_1$ | 2.021 (3) | 2.142 (4) | 2.185 (3) | 2.204 (3) |
| M1–$O3_2$ | 2.021 (3) | 2.142 (4) | 2.185 (3) | 2.204 (3) |
| $O1_1$–$O2_1$ | 2.952 (3) | 2.947 (2) | 2.939 (3) | 2.937 (3) |
| $O1_1$–$O2_2$ | 2.952 (3) | 2.947 (2) | 2.939 (3) | 2.937 (3) |
| $O1_1$–$O3_1$ | 2.533 (3) | 2.548 (3) | 2.559 (3) | 2.562 (2) |
| $O1_1$–$O3_2$ | 2.533 (3) | 2.548 (3) | 2.559 (3) | 2.562 (2) |
| $O1_2$–$O2_1$ | 2.952 (3) | 2.947 (2) | 2.939 (3) | 2.937 (3) |
| $O1_2$–$O2_2$ | 2.952 (3) | 2.947 (2) | 2.939 (3) | 2.937 (3) |
| $O1_2$–$O3_1$ | 2.533 (3) | 2.548 (3) | 2.559 (3) | 2.562 (2) |
| $O1_2$–$O3_2$ | 2.533 (3) | 2.548 (3) | 2.559 (3) | 2.562 (2) |
| $O2_1$–$O2_2$ | 2.581 (2) | 2.592 (3) | 2.618 (2) | 2.655 (2) |
| $O2_1$–$O3_1$ | 2.522 (2) | 2.539 (2) | 2.532 (2) | 2.526 (3) |
| $O2_2$–$O3_2$ | 2.522 (2) | 2.539 (2) | 2.532 (2) | 2.526 (3) |
| $O3_2$–$O3_1$ | 3.422 (4) | 3.457 (3) | 3.489 (3) | 3.494 (4) |
| $O2_1$–M1–$O2_2$ | 86.19 (3)° | 91.81 (2)° | 94.02 (3)° | 95.50 (4)° |
| $O2_2$–M1–$O3_2$ | 81.77 (4)° | 81.46 (4)° | 80.56 (3)° | 79.90 (4)° |
| $O3_2$–M1–$O3_1$ | 104.85 (4)° | 100.82 (4)° | 99.94 (2)° | 99.30 (4)° |
| $O3_1$–M1–$O2_1$ | 82.21 (3)° | 82.86 (3)° | 82.37 (3)° | 81.97 (3)° |
| $O1_1$–M1–$O1_2$ | 115.68 (4)° | 113.02 (3)° | 112.26 (4)° | 111.79 (4)° |

The relatively large number of crystal structure models for $Al_2TiO_5$ in the literature necessitated a step-by-step analysis of each model with respect to the XRD data. From this analysis, the space-group of $Al_2TiO_5$ was accepted as *Cmcm*. The index-

Table 8
Interatomic distances and angles for the M2 octahedra of $Al_2TiO_5$ at room temperature, 400, 800 and 1200 °C

| | Room temperature (Å) | 400 °C (Å) | 800 °C (Å) | 1200 °C (Å) |
|---|---|---|---|---|
| M2–$O1_1$ | 2.013 (2) | 2.054 (3) | 2.105 (3) | 2.186 (3) |
| M2–$O2_1$ | 1.874 (2) | 1.897 (3) | 1.881 (2) | 1.937 (3) |
| M2–$O2_2$ | 1.952 (3) | 1.952 (2) | 1.932 (2) | 1.874 (2) |
| M2–$O3_1$ | 2.062 (2) | 2.052 (3) | 2.071 (3) | 2.044 (4) |
| M2–$O3_2$ | 1.838 (2) | 1.836 (3) | 1.845 (3) | 1.851 (3) |
| M2–$O3_3$ | 1.838 (2) | 1.836 (3) | 1.845 (3) | 1.851 (3) |
| $O3_2$–$O1_1$ | 2.532 (3) | 2.548 (3) | 2.559 (2) | 2.563 (3) |
| $O3_2$–$O3_1$ | 2.554 (2) | 2.558 (2) | 2.550 (3) | 2.576 (2) |
| $O3_2$–$O2_1$ | 2.880 (2) | 2.886 (3) | 2.906 (3) | 2.925 (2) |
| $O3_2$–$O2_2$ | 2.857 (3) | 2.868 (3) | 2.877 (3) | 2.885 (2) |
| $O3_3$–$O1_1$ | 2.532 (3) | 2.548 (3) | 2.559 (2) | 2.563 (3) |
| $O3_3$–$O3_1$ | 2.554 (2) | 2.558 (2) | 2.550 (3) | 2.576 (2) |
| $O3_3$–$O2_1$ | 2.880 (2) | 2.886 (3) | 2.906 (3) | 2.925 (2) |
| $O3_3$–$O2_2$ | 2.857 (3) | 2.868 (3) | 2.877 (3) | 2.885 (2) |
| $O2_1$–$O1_1$ | 3.031 (2) | 3.062 (3) | 3.101 (3) | 3.146 (3) |
| $O1_1$–$O3_1$ | 3.164 (3) | 3.181 (2) | 3.195 (2) | 3.236 (2) |
| $O3_1$–$O2_2$ | 2.522 (3) | 2.539 (2) | 2.531 (2) | 2.526 (3) |
| $O2_2$–$O2_1$ | 2.405 (3) | 2.429 (2) | 2.446 (2) | 2.468 (3) |
| $O2_2$–M2–$O2_1$ | 80.56 (2)° | 80.86 (2)° | 82.18 (2)° | 82.71 (2)° |
| $O2_1$–M2–$O1_1$ | 98.22 (2)° | 97.71 (2)° | 98.12 (3)° | 96.45 (3)° |
| $O1_1$–M2–$O3_1$ | 97.71 (3)° | 97.40 (3)° | 96.34 (3)° | 96.17 (2)° |
| $O3_1$–M2–$O2_2$ | 80.61 (3)° | 81.31 (3)° | 81.14 (3)° | 82.73 (2)° |
| $O3_2$–M2–$O3_3$ | 117.47 (2)° | 117.50 (3)° | 116.88 (2)° | 116.48 (2)° |

ing of the diffraction lines in the XRD pattern, after least squares refinement using PCPIRUM, allowed the extraction of refined unit-cell parameters for the crystal system. The refined unit-cell parameters, $a = 3.593(2)$ Å, $b = 9.433(1)$ Å and $c = 9.641(1)$ Å, compare favourably with those proposed by Morosin and Lynch.[6]

Rietveld refinement of both the X-ray and neutron data allowed the optimisation of the structure parameters associated with the $Al_2TiO_5$ crystal. The use of ND data for the refinement of the crystal structure has allowed the optimisation of the site occupancy factors, especially those of the M1(Ti/Al) and M2(Ti/Al) metal sites. The values obtained for the atomic positional coordinates agree well with those proposed by Morosin and Lynch. There is however, a discrepancy between their reported site occupancy factors and those obtained from this study. Morosin and Lynch reported the M1 and M2 sites as being a mixed occupancy of Ti and Al atoms with values of 33% and 67%, respectively. This is in contrast to the values for the site occupancies obtained in this study, 41.2% and 58.8% for the Ti and Al atoms in the M1 site, and 28.8% and 71.2% for Ti and Al, respectively in the M2 site. In their work on the crystal structure of $Al_2TiO_5$, Morosin and Lynch did not refine the occupancy parameters, instead they set the values to stoichiometric and used a least squares fitting method to determine the goodness of fit. They continued this process until the goodness of fit parameter was a minimum. The final step in the optimisation of the crystal structure model of $Al_2TiO_5$ was a simultaneous refinement of both the X-ray and neutron data. The net effect of this simultaneous refinement of the data on the structure model was a substantial reduction in the standard deviations associated with each of the parameters and a very slight change in the metal site occupancy factors.

Neutron diffraction data was collected at elevated temperatures and refined using the Rietveld method. The interesting point in this series of refinements was that as the temperature was increased from 800 to 1200 °C, there is a relatively large increase of Al site occupancies in both the M1 and M2 sites. The site occupancies of Al increased from 67.8% to 71.5% for the M1 site and 69.7% to 73.3% for the M2 site. The changes in Al and Ti sites may indicate that these are "pre-transformation" or pre-eutectoid changes at the atomic scale that may enhance subsequent eutectoid decomposition on cooling. It is also interesting to note that this increase in the occupancy of the Al atoms and the temperature range over which it occurs coincides with the temperature range over which $Al_2TiO_5$ decomposes to its constituent materials, i.e. α-alumina and rutile. This is accompanied by an expansion of the unit-cell of $Al_2TiO_5$ as the temperature is increased. It is proposed that, as the material is heated through this temperature range, the crystal system contracts, so much so that it effectively ejects the Ti atom from the structure leaving the aluminium in place to form α-alumina.

The effect of temperature on the unit-cell parameters of $Al_2TiO_5$ was also examined and it was found that as the temperature increases, the *a* lattice parameter contracts. When the incremental change in lattice parameters as a function of temperature is plotted, it is found that the crystal exhibits three distinct thermal expansion coefficients, which leads to the high degree of thermal anisotropy that $Al_2TiO_5$ exhibits. The values obtained for the three thermal expansion coefficients agree well with those reported by other researchers.[6,28–30]

When looking at the structure of $Al_2TiO_5$, it is found that the crystal is composed of two distorted [$MeO_6$] octahedral units, with six oxygen atoms surrounding each metal site. These octahedra form continuous chains that are strongly bonded by apex sharing of the oxygen atom along the *a* lattice direction. These chains are then relatively weakly bonded together by edge sharing in the *bc* lattice plane. This is consistent with the observations made by Morosin and Lynch, where in their structure model, the octahedral units formed infinite chains along the *c* lattice direction and weak bonding along the shared edges in the *ab* lattice plane.

The relationship was investigated between lattice constants and thermal stability of $Al_2TiO_5$. Through studying the variation of lattice constants of $Al_2TiO_5$ with temperature, the authors discovered an abnormal phenomenon that lattice constant *c* of $Al_2TiO_5$ decreases with the increase of temperature. The authors proposed that the thermal stability of $Al_2TiO_5$ is closely related to its lattice constant *c*. The stability of $Al_2TiO_5$ can be reflected by its lattice constant *c*. The larger lattice constant *c*, the more stable $Al_2TiO_5$. Lattice constant *c* corresponds to the height of the distorted [$MeO_6$] octahedra in the crystal structure of $Al_2TiO_5$ and its increase will lead to a reduction of distortion of the octahedra, so that the stability of $Al_2TiO_5$ is improved. The effect of firing process on lattice constants and stability of $Al_2TiO_5$ was also explored. The result shows that with increase of firing temperature and extension of soaking time, $Al_2TiO_5$ exhibits larger lattice constant *c* and its stability increases correspondingly.[31]

## 5. Conclusions

The use of simultaneous refinement of the X-ray and neutron data has resulted in the improvement of the structure model for $Al_2TiO_5$. In addition, structural values of $Al_2TiO_5$ such as atomic coordinates, site occupancies and unit-cell parameters have improved. High-temperature ND studies of the $Al_2TiO_5$ crystal structure revealed an increasing substitution of Al for the Ti atoms in the crystal structure. It follows that the tyranny of the ubiquitous spontaneous decomposition of $Al_2TiO_5$ in the reported temperature range 900–1280 °C may be related to this increased substitution and the process is accompanied by an expansion of the unit-cell of $Al_2TiO_5$ as the temperature is increased.

## Acknowledgments

This work was supported by the Australian Institute of Nuclear Science and Engineering (AINSE Award No. 04/207). We thank Dr. Brett Hunter of ANSTO for experimental assistance in the collection of MRPD data.

## References


1. Dworak, W. and Fingerle, D., Ceramic materials for engines. *Br. Ceram. Trans. J.*, 1987, **86**, 170–178.
2. Stingl, P., Heinrich, J. and Huber, J., Properties and application of aluminium titanate components. In *Proceedings of the Second International Symposium on Ceramic Materials and Components for Engines*, ed. W. Bunk and H. Hausner. DKG, Bad Honnef, Germany, 1986, pp. 369–380.
3. Hennicke, H. W. and Lingenberg, W., Dependence of microstructure and physical properties of materials on the basis of aluminium titanate. In *Proceedings of the Second International Symposium on Ceramic Materials and Components for Engines*, ed. W. Bunk and H. Hausner. DKG, Bad Honnef, Germany, 1986, pp. 619–623.
4. Coor, D., Application of aluminium titanate as thermocouple protection tubes in the molten aluminium industry. *Ceram. Trans.*, 1995, **52**, 247–254.
5. Austin, A. E. and Schwartz, C. M., The crystal structure of aluminium titanate. *Acta Crystallogr.*, 1953, **6**, 812–813.
6. Morosin, B. and Lynch, R. W., Structure studies on $Al_2TiO_5$ at room temperature and at 600 °C. *Acta Crystallogr. B*, 1972, **28**, 1040–1046.
7. Epicier, T., Thomas, G., Wohlfromm, H. and Moya, J. S., High resolution electron microscopy study of the cationic disorder in $Al_2TiO_5$. *J. Mater. Res.*, 1991, **6**, 138–145.
8. Grimes, R. W. and Pilling, J., Defect formation in β-$Al_2TiO_5$ and its influence on structure stability. *J. Mater. Sci.*, 1994, **29**, 2245–2249.
9. Thomas, H. A. J. and Stevens, R., Aluminium titanate—a literature review. Part 1. Microcracking phenomena. *Br. Ceram. Trans. J.*, 1989, **88**, 44–90.
10. Thomas, H. A. J. and Stevens, R., Aluminium titanate—a literature review. Part 2. Engineering properties and thermal stability. *Br. Ceram. Trans. J.*, 1989, **88**, 184–190.
11. Kato, E., Daimon, K. and Kobayashi, Y., Decomposition temperature of β-$Al_2TiO_5$. *J. Am. Ceram. Soc.*, 1980, **63**, 355–356.
12. Kato, E., Daimon, K. and Kobayashi, Y., Factors affecting decomposition rate of $Al_2TiO_5$. *J. Ceram. Soc. Jpn.*, 1978, **86**, 626–631.
13. Kameyama, T. and Yamaguchi, T., Kinetic studies on the eutectoid decomposition of $Al_2TiO_5$. *J. Ceram. Soc. Jpn.*, 1976, **84**, 589–593.
14. Freudenberg, B. and Mocellin, A., Aluminum titanate formation by solid-state reaction of coarse $Al_2O_3$ and $TiO_2$ powders. *J. Am. Ceram. Soc.*, 1988, **71**, 22–28.
15. Buscaglia, V. and Nanni, P., Decomposition of $Al_2TiO_5$ and $Al_{2(1-x)}Mg_xTi_{(1+x)}O_5$ ceramics. *J. Am. Ceram. Soc.*, 1998, **81**, 2645–2653.
16. Ishitsuka, M., Sato, T., Endo, T. and Shimada, M., Synthesis and thermal stability of $Al_2TiO_5$ solid solutions. *J. Am. Ceram. Soc.*, 1987, **70**, 69–71.
17. Tilloca, G., Thermal stabilization of $Al_2TiO_5$ and properties of $Al_2TiO_5$ solid solutions. *J. Mater. Sci.*, 1991, **26**, 2809–2814.
18. Low, I. M., Lawrence, D. and Smith, R. I., Factors controlling the thermal stability of $Al_2TiO_5$ in vacuum. *J. Am. Ceram. Soc.*, 2005, **88**, 2940–2957.
19. Low, I. M., Oo, Z. and O'Connor, B. H., Effect of atmospheres on the thermal stability of $Al_2TiO_5$. *Physica B*, 2006, 385–386, 502–504.
20. Low, I. M. and Oo, Z., In-situ diffraction study of self-recovery in $Al_2TiO_5$. *J. Am. Ceram. Soc.*, 2008, **91**, 1027–1029.
21. Werner, P. E., *Arkiv Kemi*, 1996, **31**, 513–518.
22. DeWolff, P. M., A simplified criterion for the reliability of a powder pattern indexing. *J. Appl. Crystallogr.*, 1968, **1**, 108–115.
23. Smith, G. S. and Snyder, R. L., *J. Crystallogr. Appl.*, 1979, **12**, 60–68.
24. Hill, R. J. and Howard, C. J., *LHPM Rietveld Refinement Program Manual. Australian Atomic Energy Commission*. Lucas Heights Research Laboratory, Menai, NSW, 1986.
25. Wiles, D. B. and Young, R. A., A new computer program for Rietveld analysis of X-ray powder diffraction patterns. *J. Appl. Crystallogr.*, 1981, **14**, 149–155.
26. Penfold, D. W. and Dacombe, M. H., ed., *International Tables for Crystallography*. 2nd ed, 1987 [Revised].
27. Skala, R.D., Ph.D. Thesis, Curtin University of Technology, Perth, WA, Australia, 2001.
28. Buessem, W. R. and Gruver, R. M., *J. Ceram Am. Soc.*, 1972, **55**, 101–106.
29. Bayer, G., *J. Less-Common Metal*, 1971, **24**, 129–134.
30. Freudenberg, B., In *Concise Encyclopedia of Advanced Ceramic Materials*, ed. R. J. Brook. Pergamon Press, Oxford, 1991, pp. 20–23.
31. Jiang, W. H., Xiao, X. C., Zhou, J. E., Ma, G. H., Gu, X. Y. and Hu, X. F., Effect of variation of lattice constants on the thermal stability of $Al_2TiO_5$. *J. Inorg. Mater.*, 2000, **15**, 167–168.